

A&A manuscript no.
(will be inserted by hand later)

Your thesaurus codes are:
11(11.05.2; 11.11.1; 11.14.1; 11.16.2; 11.19.6)

ASTRONOMY
AND
ASTROPHYSICS
1.8.2018

Counter-rotating bars within bars

D. Friedli

Observatoire de Genève, CH-1290 Sauverny, Switzerland

Received 23 November 1995 / Accepted 2 February 1996

Abstract. The dynamical stability and evolution of disc galaxies with different disc thickness as well as various fraction and concentration of stellar counter-rotation is investigated with self-consistent numerical simulations. In particular, systems of nested, counter-rotating, stable bars are presented. As for the direct case, the nuclear secondary bar rotates faster than the primary bar. Contrary to the direct case, the presence of significant amount of gas is not necessary to produce such system. Observed bars within bars in lenticular (i.e. gas-poor) galaxies could thus be explained by counter-rotating bars. This hypothesis can easily be tested since the retrograde case produces distinct kinematical signatures from the direct one. Moreover, the best morphological similarities between numerical models and typical SB0's are found in the models with significant amount of stellar nuclear counter-rotation.

Key words: Galaxies: evolution – Galaxies: kinematics and dynamics – Galaxies: nuclei – Galaxies: peculiar – Galaxies: structure

1. Introduction

Among all the eccentric species observed in the zoo of galaxies, the “bar-within-bar” one (i.e. a secondary nuclear bar embedded in a primary bar) is strange enough to draw astronomer's attention (e.g. de Vaucouleurs 1974, 1975; Buta & Crocker 1993; Friedli & Martinet 1993; Shaw et al. 1993, 1995; Wozniak et al. 1995; Friedli 1996; Friedli et al. 1996). In particular, these systems have been proposed as a possible mechanism for gas fueling in active galactic nuclei (Shlosman et al. 1989, 1990). Numerous galaxies with misaligned nested stellar bars have been observed over the years by different authors in barred spirals or lenticulars suggesting a healthy population.

Various explanations can be given for the existence of such shapes: i) Projection effect of two perpendicular stellar bars. This cannot explain the small angles between the two bars observed in some almost face-on galaxies. ii) Real misalignment of two stellar bars with the same pattern speed. A very short lifetime is expected since strong gravitational torques will quickly align the two bars. iii) Action of a massive central leading gaseous bar onto stars (Shaw et al. 1993). This cannot explain the existence of both leading and trailing secondary bars (Buta & Crocker 1993; Wozniak et al. 1995). iv) Real misalignment of two stellar bars with two *different* pattern speeds but

the *same* direction of rotation. This nicely solves all the above problems. Moreover, Friedli & Martinet (1993; see also Combes 1994) have demonstrated with their self-consistent 3D N-body simulations with gas and stars that such systems can exist and be stable over many bar rotations. In this scheme, the significant primary bar-driven gas fueling plays a key role to trigger a dynamical decoupling of the central regions which start to rotate faster and independently. v) Real misalignment of two stellar bars with two *different* pattern speeds but the *opposite* direction of rotation as already simulated in 2D by Davies & Hunter (1995, 1996) and in 3D by Friedli (1996). Contrary to explanations iii) or iv), large amounts of gas are not needed in this case. If a secondary bar can easily rotate in the opposite way in comparison with a primary bar in a purely collisionless system, this mechanism could then be relevant for the gas-poor lenticular galaxies. I thus suggest that the secondary bar could counter-rotate in some (if not all) of these galaxies.

Below are presented various detailed numerical simulations of the dynamical evolution of disc galaxies with various fraction and concentration of stars in counter-rotation. Of particular interest are the models of nested, counter-rotating, stable bars. Complete formation models of such galaxies are deferred to a subsequent paper; the aim here is only to demonstrate that such systems can exist, be long-lived, and to have some insight on how they look. At first sight, this could appear as a purely academic exercise but the discovery of galaxies with massive counter-rotating stellar discs (NGC 4550, Rubin et al. 1992, Rix et al. 1992; NGC 7217, Kuijken 1993, Merrifield & Kuijken 1994; NGC 3593, Bertola et al. 1996), or gaseous discs (NGC 3926, Ciri et al. 1995; see Galletta 1996 for a recent review) raises also the general interesting question of retrograde dynamics (e.g. Levison et al. 1990; Sellwood & Merritt 1994). Moreover, a large fraction of luminous elliptical galaxies contain kinematically decoupled, counter-rotating, peculiar cores as well (see e.g. Bender 1995). Anyway, satellites on retrograde orbits exist and by dynamical friction some of them should have been swallowed by their host galaxies in the past, and have thus brought fresh retrograde angular momentum into the disc system. The formation of massive counter-rotating disks in spiral galaxies has been recently investigated by Thakar & Ryden (1995).

This paper is constructed as follows: The code, the models and the definitions used are given in Sect. 2. Section 3 briefly recalls the results obtained in the direct cases whereas Sect. 4 presents in a detailed way the formation, evolution, morphology and kinematics of the retrograde cases. A general discus-

sion as well as possible formation scenarios are presented in Sect. 5 and my conclusions are summarized in Sect. 6.

2. Code, models and definitions

2.1. The code

Our self-consistent 3D simulations of disc galaxies are modeled with a purely collisionless component (stars) as well as with a dissipative one (gas) in some models. The complete code description is given in Pfenniger & Friedli (1993) for the gravitational part (Particle-Mesh method), and in Friedli & Benz (1993) for the hydrodynamical part (Smooth Particle Hydrodynamics technique). Typically, the number of star particles is $2 \cdot 10^5$ and the number of gas particles, when present, is $1 \cdot 10^4$. The time integration is performed with a leap-frog algorithm (constant time-step $\Delta t = 0.25$) in purely collisionless systems and with a Runge-Kutta algorithm (adaptive time-step) in mixed systems with gas and stars.

2.2. Models

Initially, the models are axisymmetric. Their stellar parts are distributed according to a superposition of two Miyamoto-Nagai models of mass M_1 and M_2 , with vertical scale-heights b_1 and b_2 , and horizontal scales $a_1 + b_1$, $a_2 + b_2$; the mass of the gaseous disc is M_g (for details see Friedli & Benz 1993). The rotation velocity and the three components of the velocity dispersion are numerically computed on the grid so as to satisfy the equilibrium solutions of the stellar hydrodynamical equations. The systematic rotation velocity of the component 1 can be put either like the one of the component 2 (direct models D_i) or in the opposite direction (retrograde models R_i). Obviously, this does not correspond to a very realistic formation scheme, but the aim here is mainly to prove that such configurations can exist and be stable. A discussion concerning complete formation scenarios is given in Sect. 5.

2.3. Units and definitions

For computational convenience, the calculations are performed in units suitable for galactic problems. The unit length is chosen to be the kpc, the unit mass represents $2 \cdot 10^{11} M_\odot$, and with $G=1$ the time unit is 1.05 Myr.

The bar with the smaller extent will be referred as the “secondary bar” and all the quantities related with it will have the subscript s . The bar with the larger extent will be referred as the “primary bar” and all the quantities related with it will have the subscript p . Thus, for instance the primary and secondary bar maximum ellipticities are respectively denoted as e_p^{\max} and e_s^{\max} . These values are determined with the ellipse fitting technique (for details see Wozniak et al. 1995). The angle between the two bars is θ . Positive values are for leading secondary bars whereas negative values are for trailing secondary bars (relative to the primary bar rotation). The other quantities are:

- The ratio $\alpha \equiv \Omega_s/\Omega_p$, where the Ω_i are the bar pattern speeds.
- The ratio $\beta \equiv l_p/l_s$, where the l_i are the bar lengths.
- The ratio $\gamma \equiv m_p/m_s$, where m_s is the total mass between the centre and l_s , and m_p is the total mass between the centre and l_p .

3. The direct models

3.1. Fast nested bars within bars ($\beta > 1$, $\alpha > 1$)

This direct case has extensively been discussed and described in Friedli & Martinet (1993) so that only a brief summary is given here. The basic model D_1 has the following initial parameters: $M_g = 0.1$, $M_1 = 0.1$, $M_2 = 0.8$, $a_1 = b_1 = 0.2$, $a_2 = 6.0$, and $b_2 = 0.75$. The initial stellar rotation curve is given in Fig. 1a.

Schematically, the general evolution of the simulation is: 1) Slow and simultaneous formation of the primary and the secondary bar (i.e. $\beta > 1$). 2) Phase of two bars with different pattern speeds (i.e. $\alpha > 1$) due to a decoupling of the central dynamics from the outer parts. Progressive formation of a nuclear gaseous ring near the corotation radius CR_s . 3) Dissolution of the secondary bar, the primary bar remains with the nuclear ring anti-aligned with it. The central gaseous mass accreted is not sufficient to dissolve the primary bar as well. The appearance of a double-barred system and a nuclear gaseous ring are favoured by the following characteristics: 1) The two stellar discs must obviously be bar unstable and the primary bar must have an inner Lindblad resonance (ILR) allowing for the presence of the anti-bar x_2 orbit family which is essential for increasing the efficiency of the decoupling. 2) To maintain the dynamical decoupling¹, a significant dissipative component has to be present. Then the material, which accumulates onto the central galaxy part, reinforces the secondary bar strength, and prevents the fast slow down of its pattern speed. 3) Systems with $\alpha \gg 1$ minimize the interaction between the two bars and those with the CR_s coincident with the ILR_p minimize the generation of chaos. 4) Slow enough bar growth(s) and not too strong bar strength(s) are favourable for the formation of a nuclear gaseous ring during the two bar phase. This indeed insures that some gas remains outside the secondary bar region.

At $t = 1200$, this double-barred model has the following characteristics: $\alpha \approx 3.1$, the positions of the axisymmetric ILR_p and CR_s are about the same, $\theta \approx 90^\circ$, $\beta \approx 5.4$, $\gamma \approx 2.9$, $e_s^{\max} \approx 0.39$, and $e_p^{\max} \approx 0.27$. Different values have also been obtained in new recent simulations (Friedli et al. 1996). The stellar rotation curve is shown in Fig. 1b.

3.2. Leading nested bars within bars ($\beta > 1$, $\alpha = 1$, $+10^\circ \lesssim \theta \lesssim +80^\circ$)

Shaw et al. (1993) have presented models with gas and stars which produce two misaligned stellar bars rotating at the same pattern speed. First the star-gas disc is unstable and quickly forms a primary bar with two ILR’s. The gas clouds should follow the x_2 family but due to dissipative collisions they are in fact gradually shifted from parallel to perpendicular orbits relative to the primary bar and the gas settles in a *leading* phase-shifted bar. If the gas fraction is high, its gravitational influence is then sufficient to modify the stellar component itself and to form the secondary stellar bar. Combes (1994) indicates $\theta \approx +30^\circ$ but in principle angles $+10^\circ \lesssim \theta \lesssim +80^\circ$ are possible depending on the model properties, in particular its viscosity. Unfortunately, this model cannot account for the existence of observed *trailing* secondary bars.

¹ The dynamical *decoupling* could be related to non-linear mode *coupling* (Tagger et al. 1987)

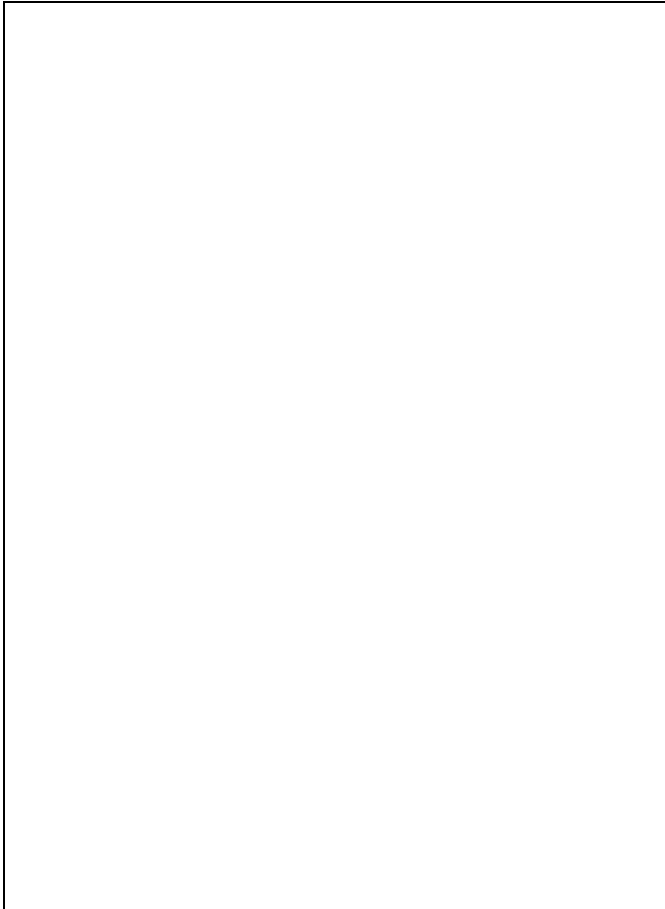


Fig. 1a and b. Systematic, azimuthally averaged, tangential velocity V_t as a function of radius for models D_1 (dashed-dotted curve), R_1 (dotted curve), R_2 (dashed curve), and R_3 (solid curve). **a** $t=0$, and **b** $t=2000$ for the retrograde models and $t=1200$ for the direct model

It is not yet clear what allows some galaxies to have one single pattern speed and other to have two different pattern speeds. In both cases, the gas-star coupling is essential. Simulations by Combes (1994) seem to indicate that the gas viscosity plays the determining role: Systems with high viscosity tend to decouple and form two independent bars whereas systems with low viscosity preferentially form a phase-shifted secondary bar.

4. The retrograde models

4.1. Nearly perpendicular nested bars within bars ($\beta > 1$, $\alpha = 1$, $\theta \approx -80^\circ$)

The model R_1 has the following initial parameters: $M_g = 0.0$, $M_1 = 0.2$, $M_2 = 0.8$, $a_1 = 1.0$, $a_2 = 6.0$, $b_1 = b_2 = 0.75$. The retrograde component represents 25% of the mass of the direct component but only about 5.7% of the angular momentum (in absolute value). The counter-rotating component is not strongly centrally concentrated and the systematic tangential velocity V_t is only slightly negative near the centre (see Fig. 1a).

The time evolution of this model is presented in Fig. 2. A prominent bar quickly develops in the direct disc. This primary

bar (sustained by the x_1 periodic orbit family) totally dominates the dynamics so that the retrograde disc is first essentially influenced by the x_4 2D periodic orbit family, and then around $t = 2000$ by the anomalous 3D periodic orbit family which bifurcates from the x_4 (1/1 vertical resonance). These families are slightly anti-bar so that the retrograde disc becomes weakly barred. This bar is always nearly perpendicular to the primary bar but remains almost indistinguishable when the total surface density is plotted (nearly round centre). The bar looks very nicely like typical SB0's, i.e. the isodensity contours are round near the centre, then take the shape of an elongated hexagon, and finally become close to rectangular.

Both bars have the same pattern speed ($\approx 20 \text{ km s}^{-1} \text{ kpc}^{-1}$). Thus, *the secondary bar pattern rotates in the opposite direction in comparison with the stars which compose it!* This system lasts about 2 Gyr. At $t = 3000$ about 58% of the angular momentum of the retrograde component has however been transferred. As a consequence, the retrograde component becomes nearly spherical and V_t is no more negative near the centre (see Fig. 1b). At $t = 2000$, this double-barred model has the following characteristics (total surface density): $\alpha \approx 1.0$, $\theta \approx -75^\circ$, $\beta \approx 16.4$, $\gamma \approx 12.5$, $e_s^{\text{max}} \approx 0.25$, and $e_p^{\text{max}} \approx 0.58$. This corresponds to the time where the secondary bar is the strongest. By comparison, $e_s^{\text{max}} \approx 0.12$ at $t = 1500$ and $e_s^{\text{max}} \approx 0.10$ at $t = 3000$ whereas e_p^{max} keeps about the same value. The secondary bar length l_s is also decreasing from 0.85 kpc at $t = 1500$ to 0.49 kpc at $t = 3000$.

The same model but with low initial disc thickness is strongly unstable with respect to central bar and bending modes. Then, after the quick dissolution of the counter-rotating component (due to the cancelation of its retrograde angular momentum approximately twice faster than in model R_1), this model evolves like model R_1 .

4.2. Slow large-scale bars within bars ($\beta = 1$, $\alpha = -1$)

The model R_2 has the following initial parameters: $M_g = 0.0$, $M_1 = 0.5$, $M_2 = 0.5$, $a_1 = a_2 = 6.0$, $b_1 = b_2 = 0.25$. So, this corresponds to two identical thin discs which rotate in the opposite way, very similar to what can be observed in the edge-on galaxy NGC 4550 (Rubin et al. 1992; Rix et al. 1992). The total angular momentum is zero as well as the systematic tangential velocity (see Fig. 1a).

As studied by Sellwood & Merritt (1994), this kind of very flat, counter-rotating, disc system is strongly unstable with respect to bending modes. The same authors (see also Levison et al. 1990) reported in some cases *the formation of two bars with the same extent which were rotating in the opposite direction*. This is also what I observe for this model from $t = 2000$ on (see Fig. 3): Two slowly ($\approx 18 \text{ km s}^{-1} \text{ kpc}^{-1}$) counter-rotating weak bars which persist for at least 2 Gyr. Both discs have also a strong $m = 1$ mode. To my knowledge no face-on galaxies of this type have so far been observed in nature. This is not very surprising since the total face-on surface density does not present very specific characteristics and such systems could easily be missed without kinematic data. High initial disc thickness suppresses bending modes and counter-rotating bars.

At $t = 2000$, this double-barred model has the following characteristics: $\alpha \approx -1.0$ so that the position of resonances are identical, $\theta \approx +60^\circ$, $\beta \approx 1.0$, $\gamma \approx 1.0$, and $e_s^{\text{max}} \approx e_p^{\text{max}} \approx 0.38$. No systematic velocity develops (see Fig. 1b). The total angular

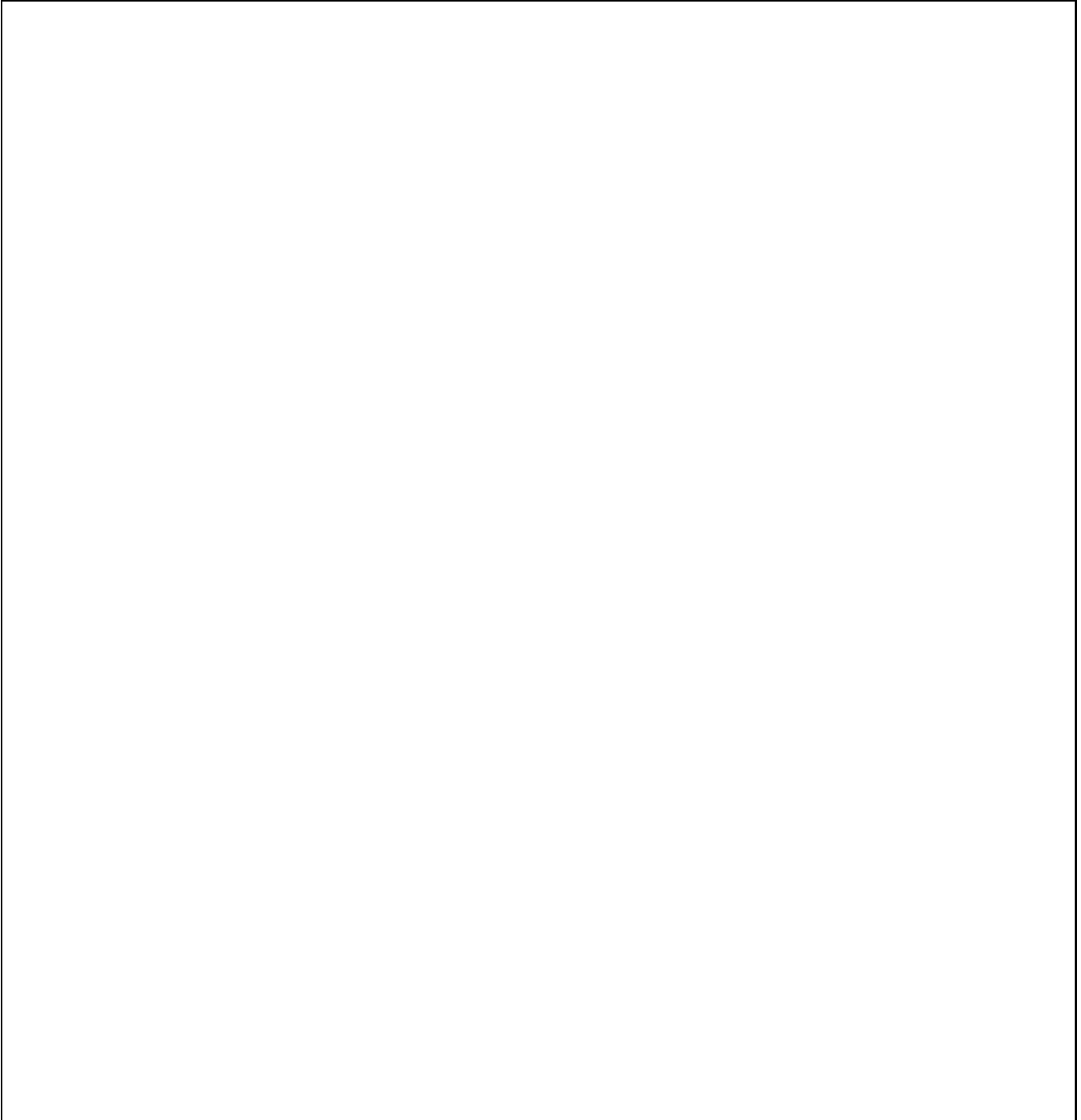


Fig. 2. Time evolution of the stellar surface density projected in the three principal planes of the model R_1 for the retrograde component with clockwise rotation (left column), the direct component with counter-clockwise rotation (middle column), and the total (right column). The side of the square frames is 10 kpc for the left column and 20 kpc for the other ones. The isodensity contours are separated by 0.3 dex. The time t is indicated at the bottom left of each frame. The rotation of the *two* bars is counter-clockwise with a rotation period of approximately 320 Myr. Note the box-peanut shape at $t=3000$

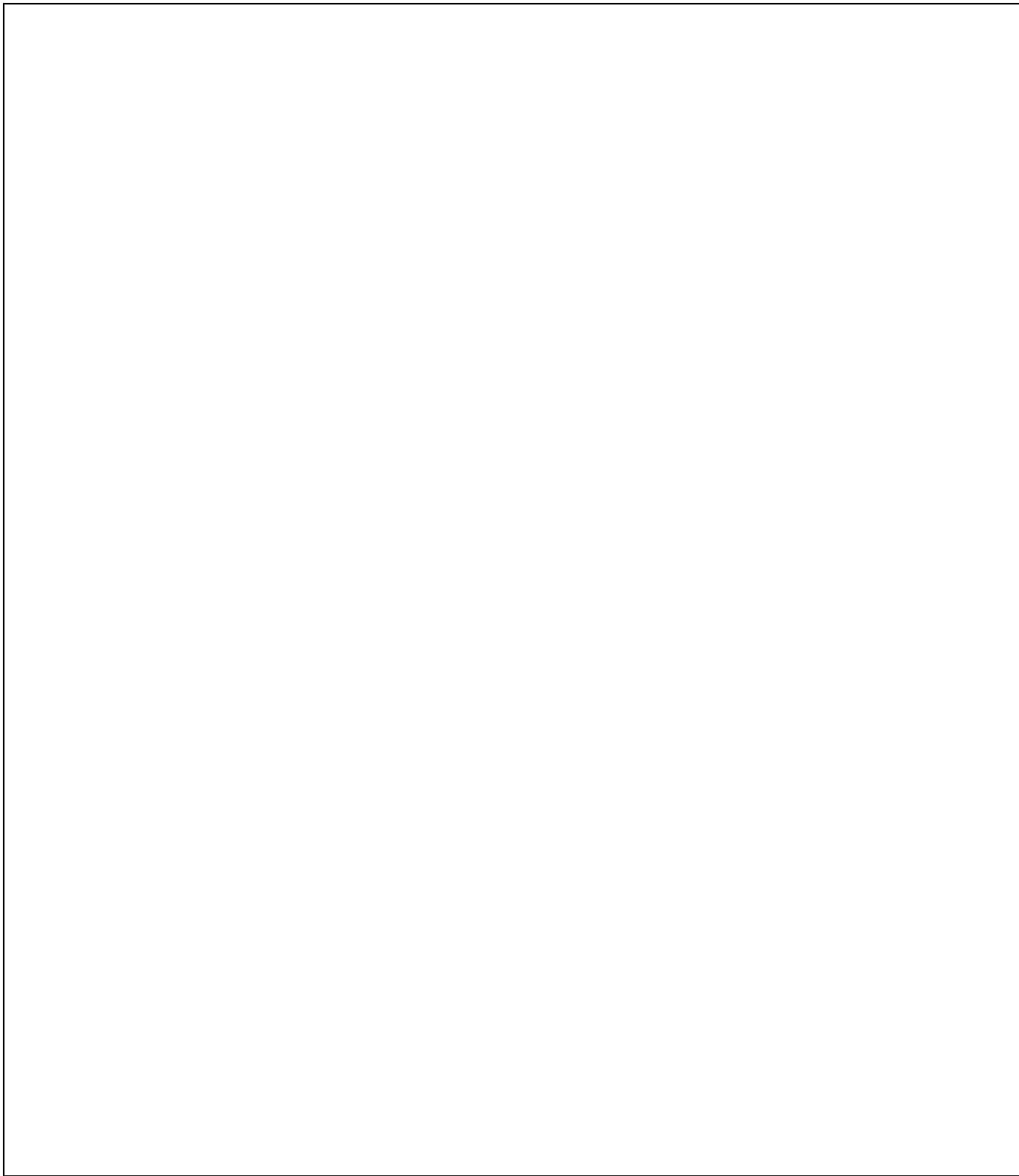


Fig. 3. The same as Fig. 2 but for the model R_2 . The retrograde bar in the left column rotates clockwise whereas the direct bar rotation in the middle column is counter-clockwise. Both rotation periods are approximately 350 Myr

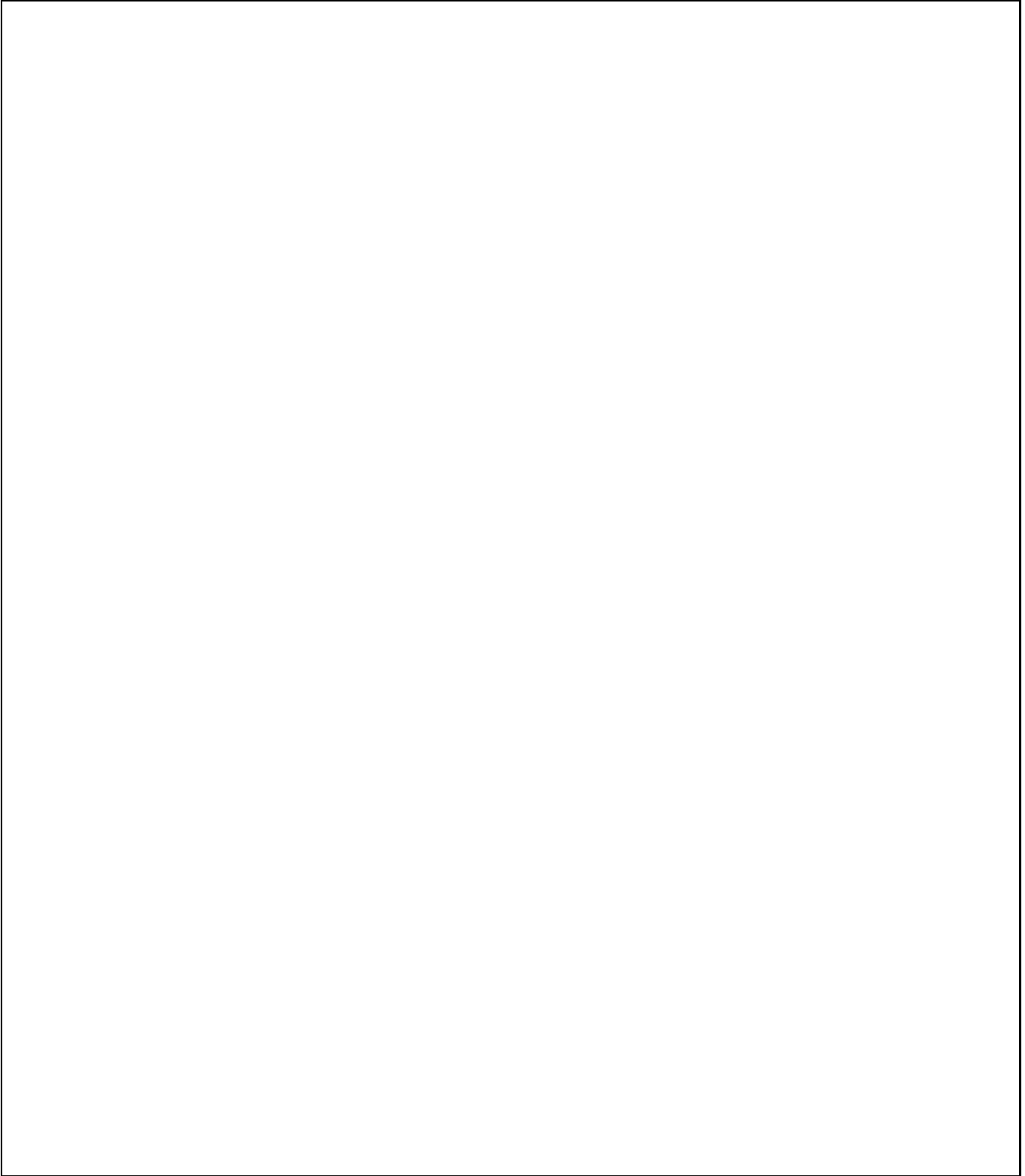


Fig. 4. The same as Fig. 2 but for the model R_3 at the beginning of the simulation, during a fraction of the two counter-rotating bar phase, and at the end of the simulation. The rotation periods are approximately 240 Myr for the large-scale primary bar (counter-clockwise rotation) and 130 Myr for the small-scale secondary bar (clockwise rotation)

momentum remains zero but those of each disc decreases by about 15%.

4.3. Fast nested bars within bars ($\beta > 1$, $\alpha < -1$)

The typical model R_3 has the following initial parameters: $M_g = 0.0$, $M_1 = 0.2$, $M_2 = 0.8$, $a_1 = b_1 = 0.4$, $a_2 = 6.0$, and $b_2 = 0.75$. The idea is to explore the viability of system with $\alpha < -1$. The counter-rotating component is strongly concentrated to prevent the direct component from dominating the central dynamics as in model R_1 . Its mass represents 25% of the mass of the direct component but only about 2.9% of the angular momentum (in absolute value). The systematic tangential velocity becomes strongly negative near the centre (see Fig. 1a). This system is similar to what can be observed in NGC 3593 (Bertola et al. 1996).

With these specific initial conditions, the two discs remain axisymmetric for 1 Gyr and then *each disc forms its own bar which rotate in the opposite direction, i.e. each bar rotates in the same way as the stars which compose it* (see Fig. 4). The secondary bar forms first (around $t = 1200$) and is faster. The existence of this central dynamical decoupling is made easier by the presence of the x_4 orbits. The lifetime of the counter-rotating nested bar phase is about 1 Gyr, i.e. approximately between $t = 1500$ and $t = 2500$. Just after $t = 2500$, the secondary bar reverses its direction of rotation, overtakes the primary bar, oscillates for some time around it and finally aligns itself with it. At $t = 3000$, the secondary bar is nearly fully dissolved into a round centre. This evolution is mainly driven by the significant angular momentum transfer between the secondary and the primary bar. Indeed, at $t = 2000$ the angular momentum of the retrograde component has already been decreased by more than 27% and then approximately three more percents are annihilated every 100 Myr.

Davies & Hunter (1995, 1996) have also studied the effects which result from putting retrograde angular momentum in galactic discs. In particular, they have presented models of counter-rotating bars within bars. They start with a single 2D disc model whose central systematic velocities are abruptly reversed. They have essentially found the same evolutionary behaviour as in my models. Zang & Hohl (1978) have shown that a large fraction of stars on retrograde orbits strongly inhibits the formation of the primary bar. Here, the growth of the primary bar is slow but it finally appears. It is not yet clear what fraction would be necessary to fully prevent the primary bar to form and if stars on retrograde orbits could easily dissolve an already formed strong bar.

The same model but with low initial disc thickness is strongly unstable with respect to central bar and bending modes; the retrograde angular momentum is very quickly cancelled out (5 times faster than in model R_3) giving rise to a one direct bar model.

4.3.1. Morphology and resonances

The morphological evolution of this model during a fraction of the two bar phase is shown in Fig. 4 for each component as well as for the addition of them. The ellipse fits at $t = 2000$ are given in Fig. 5. The total surface density features of the model are $\theta \approx -60^\circ$, $\beta \approx 4.1$, $\gamma \approx 2.4$, $e_s^{\max} \approx 0.29$, and $e_p^{\max} \approx 0.48$. These values are contained between the observed intervals (Wozniak et al. 1995; Friedli et al. 1996). The two

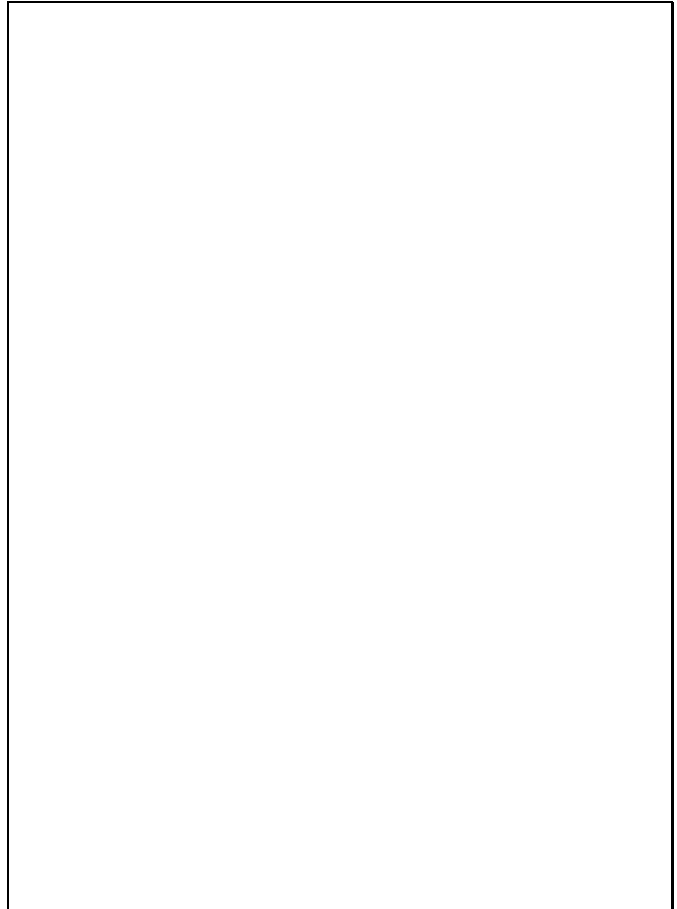


Fig. 5. Plots of stellar surface density μ , ellipticity e and position-angle PA profiles as a function of the semi-major axis of the fitted ellipse, for the total density (solid curve), the direct component only (dotted curve), and the retrograde component only up to 5 kpc (dashed curve). Model R_3 seen face-on at $t = 2000$

bars have two distinct and nearly exponential profiles whose scale-length ratio is close to 0.13. Very similar bar-within-bar morphology as the one of model R_3 have been observed in many SB0's (e.g. NGC 1291, NGC 1543). One can thus reasonably consider that some of these galaxies could host counter-rotating bars within bars.

The primary bar pattern speed is $\approx 29 \text{ km s}^{-1} \text{ kpc}^{-1}$ whereas the secondary bar one is $\approx -40 \text{ km s}^{-1} \text{ kpc}^{-1}$ giving $\alpha \approx -1.4$. So, the secondary bar does not rotate that fast, only about half the value of the direct case although both cases have similar β and γ . As a consequence and contrary to the direct case, the secondary bar does not end close to its corotation radius but near its outer ILR radius (cf. Fig. 5). Moreover, the CR_s and the ILR_p are not coincident. This seems to indicate that the formation of retrograde secondary bars is less constrained than for the direct ones. The central decoupling is indeed made easier in counter-rotation than in direct rotation, and does not require large amounts of gas. Note that the relative pattern speed between the two bars is similar for the retrograde and the direct cases (2.4 and 2.1 respectively).



Fig. 6a and b. Line-of-sight **a** velocity V_{los} , and **b** velocity dispersion σ_{los} , for model R_3 at $t=1000$ (no bars) of both components (crosses), at $t=2000$ ($\theta \approx -60^\circ$) of both components (filled circles), the direct component (open circles), and the retrograde component up to 3 kpc (open triangles). The “numerical slit” is 0.4 kpc wide and is oriented along the primary bar major axis. Models are seen edge-on

4.3.2. Kinematics

Near the centre at $t=2000$, V_t is still negative although much less than at the beginning (see Figs. 1a and b). This is a true counter-rotation. Clearly, direct and retrograde double-barred models have different V_t . Some rotation curves of SB0’s along the bar major axis show negative values near the centre (Bettoni 1989) but it is not yet clear if this is only an apparent counter-rotation due to projection effects on streaming motions or poor slit alignment with the bar major axis (see Wozniak & Pfenniger 1996 for a recent discussion of this problem).

In order to be in a position to compare numerical models with observations in a proper way, the line-of-sight velocity V_{los} and velocity dispersion σ_{los} have been computed through a “numerical slit”. Owing to the particle noise, differences depending on the slit alignment or θ are difficult to clearly highlight, so that only the most favourable situation will be analysed here, i.e. the edge-on case.

Model R_3 is displayed in Figs. 6a and b at two different times, i.e. at $t=1000$ where no bar has yet developed, and at $t=2000$ in the middle of the two counter-rotating bar phase. In the latter case, the slit is aligned along the primary bar,

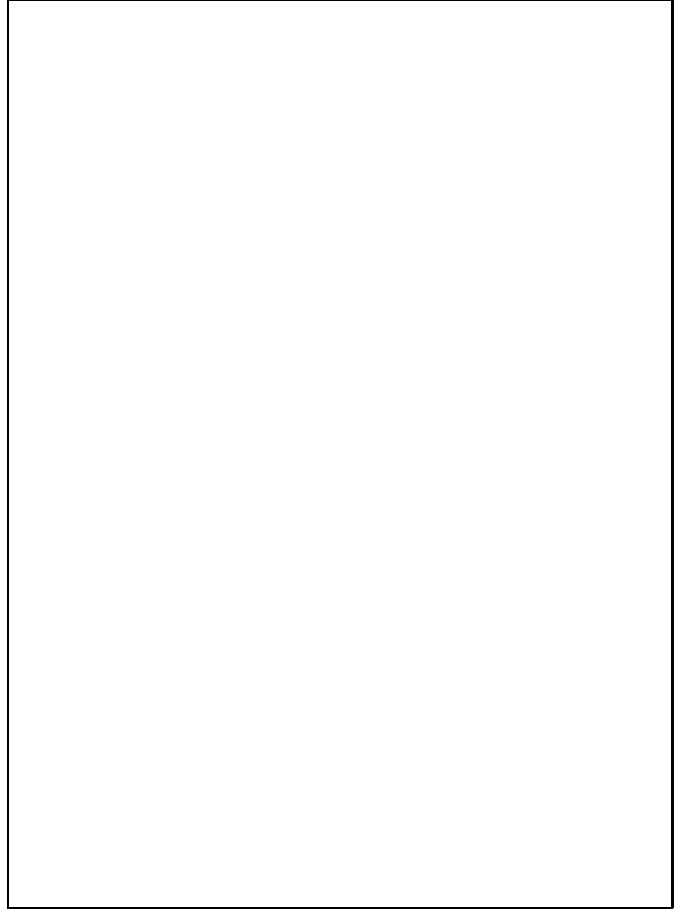


Fig. 7a and b. The same as Figs. 6a and b but for both components of model R_3 at $t=2100$ ($\theta \approx 90^\circ$) along the primary bar major axis (filled circles), along the primary bar minor axis (open circles), as well as for model D_1 at $t=1200$ ($\theta \approx 90^\circ$) along the primary bar major axis (open triangles), and along the primary bar minor axis (crosses). Models are seen edge-on

and $\theta \approx -60^\circ$. These two models have at 0.5 kpc a respective maximum net counter-rotation of $V_{\text{los}} \approx 15 \text{ km s}^{-1}$ and $V_{\text{los}} \approx 35 \text{ km s}^{-1}$. The rotation of the individual components is also shown at $t=2000$. The formation of the primary bar results in a decrease of V_{los} by a few tens of km s^{-1} beyond 2 kpc. The most spectacular effect induced by the two bar formation is observed on σ_{los} ; at $t=1000$ (as well as in the initial conditions), its profile displays a central dip of $\approx 30 \text{ km s}^{-1}$ which is almost fully erased by the secondary bar formation at $t=2000$. This model has a nearly flat profile up to 1.5 kpc ($\sigma_{\text{los}} \approx 190 \text{ km s}^{-1}$), i.e. close to l_s seen at an angle of 60° . So, the central galaxy part is considerably getting hotter with time. An even deeper dip has also been observed by Bertola et al. (1996) in NGC 3593. This is a strong indication that this galaxy has not (yet?) formed a central counter-rotating secondary or nuclear bar. The central σ_{los} of the retrograde component is $\approx 50 \text{ km s}^{-1}$ smaller (i.e. colder) than the one of the direct component.

Figures 7a and b compare models R_3 at $t=2100$ and D_1 at $t=1200$ with the slit i) aligned along the primary bar major axis, and ii) aligned along the secondary bar major axis. In both models, the primary and secondary bar are nearly per-

pendicular ($\theta \approx 90^\circ$). In the model R_3 , V_{1os} shows a maximum counter-rotation ($\approx 30 \text{ km s}^{-1}$) when the slit is aligned along the secondary bar major axis, and in this case σ_{1os} displays a distinct peak of nearly 20 km s^{-1} above the otherwise observed flat profiles. Although direct and retrograde models are not fully comparable (gas is present in the direct models), it is however instructive to highlight major differences. Models R_3 mainly differs from model D_1 by its true central counter-rotation, and by its apparent rotation around 2 kpc which is about 40 km s^{-1} slower. The apparent rotational support is thus only about 70 km s^{-1} . This is much less than the circular velocity ($\approx 310 \text{ km s}^{-1}$). The two σ_{1os} profiles are also very different. The retrograde model has either a flat profile up to 1.5 kpc, or a steeper profile with a shoulder between 1.0 and 1.5 kpc. Then σ_{1os} decreases nearly linearly. The velocity dispersion of model D_1 is very similar at the centre ($\sigma_{1os} \approx 185 \text{ km s}^{-1}$) but then steeply decreases. At 2 kpc, it is approximately 40 km s^{-1} lower than the one of model R_3 .

In the face-on case, we have $\sigma_{1os} = \sigma_z$. With time, the σ_z radial profile is progressively becoming less sharply falling. Interestingly enough, the observed profiles of the double-barred galaxies NGC 1291 and NGC 1543 by Jarvis et al. (1998) have a very slow decrease as well!

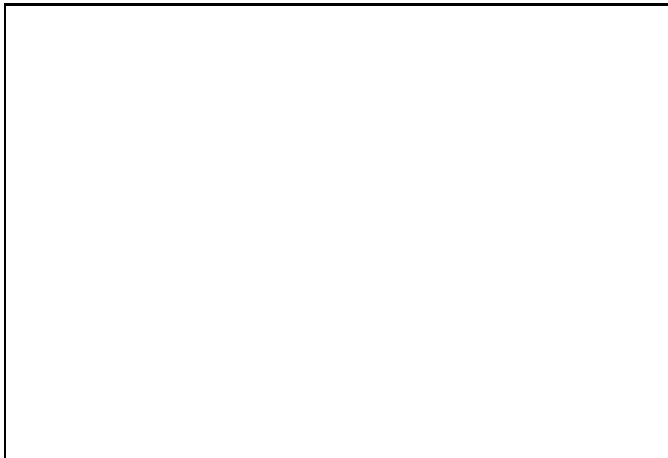


Fig. 8. Schematic sketch of the effect of disc thickness and retrograde angular momentum concentration on the galaxy stability and evolution. The position of the models discussed in Sect. 4 are indicated

In conclusion, the kinematics of counter-rotating bar-within-bar models is clearly distinct (e.g. significant central counter-rotation of V_{1os} ; flat central σ_{1os} profiles) from the one of direct bar-within-bars models. High resolution central velocity field mappings of early-type galaxies should bring the deciding proof concerning the secondary bar direction of rotation. Moreover, in highly inclined galaxies with concentrated counter-rotation (e.g. NGC 3593), one should easily distinguish between disc and bar components from kinematic features (i.e. truncated pyramid-like σ_{1os} profile or volcano-like σ_{1os} profile).

5. Discussion

The dynamical evolution of disc systems with stellar counter-rotation appears to be dependent on at least three parameters:

The disc thickness, the mass and the central concentration of the retrograde component. A schematic summary is displayed in Fig. 8. Although the whole space parameter have not yet been explored, the presence of bending instabilities are clearly dependent on the disc thickness (Sellwood & Merritt 1994). Bending modes disappear in thicker discs. In this case, the evolution is very different depending on the concentration of retrograde angular momentum (which increases when a_1 decreases and M_1 increases). A low concentration keeps the system stable and axisymmetric. An intermediate concentration leads to the formation of a dynamically-dominant direct bar whose retrograde phase-space entirely dominates the counter-rotating component. A high concentration allows the dynamical decoupling between the two components and leads to counter-rotating bars within bars.

Interestingly enough, the best morphological similarities between numerical models and typical SB0's occur in the models with significant amount of central stellar counter-rotation. Indeed, if the central part of the galaxy (the bulge) is co-rotating with the primary bar, it also cooperates with the bar instability and generally aligns with it (unless i) it is hot enough, or ii) it significantly counter-rotates (model R_1). If the central mass is high enough, a dynamical decoupling occurs both in the direct and retrograde cases leading to the formation of bars within bars systems (models D_1 and R_3). If the central mass is even higher, no bars can form. For instance, the presence of supermassive black holes in the nucleus generates very hot centres and S0-like galaxies (Friedli 1994). So, I suspect that some lenticular galaxies should have recently accumulated significant retrograde angular momentum, for instance by retrograde satellite cannibalism. Note that retrograde orbits are more stable than direct ones, and thus the fraction of retrograde to direct satellites should increase with time around galaxies. The above picture is consistent with the very high and convincing evidences for an evolution along the Hubble sequence from late-types to early-types (see e.g. Martinet 1995 and references therein). In particular, small bulges (types Sc and Sb) can form from bars, bigger bulges (types Sa and S0) can be generated by satellite accretion (Pfenniger 1993), whereas elliptical galaxies can result from the merging of two or more spirals (Barnes 1992). Another interesting point is that the presence of bars allows the progressive annihilation of the angular momentum of each component in the regions with both direct- and counter-rotation. This clearly leads to a decrease of the rotational support in favour of pressure support allowing the formation of big bulges. The central spiraling of retrograde satellites should thus trigger the formation of bigger bulges than direct ones. Distinct signs of counter-rotation will thus disappear with time and discs within discs should survive longer than bars within bars.

In Sect. 4.3, the viability of nested, counter-rotating, stable bars has been demonstrated by numerical simulations. However, the initial conditions are purely ad-hoc and certainly do not correspond to any realistic formation scenario. Indeed, the aim of this paper is not to show a complete formation sequence but only to demonstrate that such systems can exist, be long-lived, and to gain some insight on how they evolve. Three more realistic formation schemes of such systems are discussed below which will be investigated in more depth in a subsequent paper.

A. Fast accretion of a retrograde gas-poor satellite by an early-type barred galaxy. If a moderately compact and massive (5%–

15% of the host galaxy mass) gas-poor satellite on a retrograde orbit is swallowed by a barred galaxy, dynamical friction will cause it quickly to spiral to the centre and could produce there a counter-rotating secondary bar. The primary bar can already be formed or be induced by the close interaction with the satellite. No induced star formation has to be considered. There is however two major drawbacks: 1) If the satellite is very compact, the merging of the galaxy and the satellite should result in a significant dynamical heating which is able to dissolve the primary bar and prevent the secondary bar from being formed. Moreover, observations of NGC 3593, NGC 4550 and NGC 7217 indicate cold, rotationally supported, galaxies. Fast merging is unlikely to have produced these systems. In addition, other signatures of the interaction (like $m = 1$ modes, tails, ripples, etc.) should be present as well. 2) On the contrary, if the satellite is too loosely bound, it will be tidally disrupted and not enough mass will remain in the centre to produce a distinct counter-rotating component. So, a very fine tuning could be requested to produce in this way two nested counter-rotating bars.

B. Fast accretion of a retrograde gas-rich satellite by an early-type barred galaxy. In this case, the evolution proceeds similarly to the scenario A but at an expected faster rate due to significant gas-dissipation. The drawback 1) of scenario A remains. The drawback 2) of scenario A is alleviated since even if the satellite is tidally disrupted before reaching the centre, dissipation insures that the gas will first settle into the disc plane and then spiral towards the nucleus. In particular, the gas coming from mass loss due to stellar evolution in the direct component will interact with the retrograde gas and strong dissipative shocks should occur. Here, the main problem concerns the way star formation is proceeding to transform the central gas-rich component into a star-dominated one.

C. Slow accretion of retrograde gas by an early-type barred galaxy. The progressive, adiabatic, building up of a counter-rotating compact gaseous disc by continuous or episodic infall is expected to preclude excessive heating of the direct preexisting disc, removing thus the drawback 1) of scenarios A and B. Numerical simulations by Thakar & Ryden (1995) have shown that this is feasible but star formation is not yet included in their models. In the bar region, the gas should be trapped by the stable retrograde x_4 and anomalous periodic orbit families (inclined loops) which have a large extent. But again, for the most part the gas has to be transformed into stars and it is not yet clear if the counter-rotating component could concentrate enough before becoming collisionless-dominated. However, different rates of infall, initial retrograde angular momentum, star formation histories could succeed in reproducing the various types of galaxies with counter-rotation observed so far.

6. Conclusions

The main conclusions of this paper are the following:

- 1) Self-consistent collisionless disc models of embedded counter-rotating bars within bars can exist. Their lifetimes can at least reach one Gyr. Contrary to direct bars within bars models, no gas is necessary. Counter-rotating secondary bars may thus be relevant for the gas-poor double-barred early-type galaxies (e.g. NGC 1291).
- 2) The presence of counter-rotating bars within bars produces peculiar signatures in the central line-of-sight velocities of the

numerical models. The observational existence of such systems in early-type galaxies could thus be inferred through kinematic evidences. In the case of NGC 3593, the counter-rotating central component is apparently not barred.

3) The best morphological similarities between numerical models and typical SB0's occur in the models with significant amount of stellar nuclear counter-rotation. These galaxies might have either adiabatically accumulated retrograde angular momentum to the centre or recently swallowed a few retrograde satellites.

4) In case of non-axisymmetric potential, the angular momentum of each component is progressively transferred and cancelled out in the regions with both direct- and counter-rotation. So, with time the signatures of the retrograde motion will disappear and the rotational support will decrease in favour of pressure support allowing the formation of big bulges. The central spiraling of retrograde satellites should trigger the formation of bigger bulges than direct satellites.

5) Self-consistent collisionless disc models of counter-rotating bars within bars having the same mass, scale-length, axis ratio, and pattern speed can also be constructed. However, thus far no connection with any observed galaxies has been established.

Acknowledgements. This work has been supported by the University of Geneva (Geneva Observatory) and the Swiss National Science Foundation (FNRS). I especially thank H. Wozniak for having made available his ellipse fitting code as well as L. Martinet and D. Pfenniger for a careful reading of the manuscript, and the referee, J.H. Hunter, for his valuable comments. I wish also to thank C. Davies for many fruitful discussions.

References

- Barnes J.E., 1992, ApJ 393, 484
 Bender R., 1995, in: Galaxies in the Young Universe, Ed. H. Hippelein. Springer, Heidelberg, (in press)
 Bertola F., Cinzano P., Corsini E.M., et al., 1996, ApJ, (in press)
 Bettoni D., 1989, AJ 97, 79
 Buta R., Crocker D.A., 1993, AJ 105, 1344
 Ciri R., Bettoni D., Galletta G., 1995, Nat 375, 661
 Combes F., 1994, in: Mass-Transfer Induced Activity in Galaxies, ed. I. Shlosman. Cambridge University Press, Cambridge, p. 170
 Davies C.L., Hunter J.H. Jr., 1995, in: Waves in Astrophysics, eds. J.H. Hunter Jr., R.E. Wilson. New York Academy of Sciences, New York, (in press)
 Davies C.L., Hunter J.H. Jr., 1996, MNRAS, (submitted)
 de Vaucouleurs G., 1974, in: Formation of Galaxies, IAU Symp. No 58, ed. J.R. Shakeshaft. Reidel, Dordrecht, p. 335
 de Vaucouleurs G., 1975, ApJS 29, 193
 Friedli D., 1994, in: Mass-Transfer Induced Activity in Galaxies, ed. I. Shlosman. Cambridge University Press, Cambridge, p. 268
 Friedli D., 1996, in: Barred Galaxies, IAU Coll. No. 157, eds. R. Buta et al. ASP Conference Series, (in press)
 Friedli D., Benz W., 1993, A&A 268, 65
 Friedli D., Martinet L., 1993, A&A 277, 27
 Friedli D., Wozniak H., Rieke M., Martinet L., Bratschi P., 1996, A&AS, (submitted)

- Galletta G., 1996, in: Barred Galaxies, IAU Coll. No. 157, eds. R. Buta et al. ASP Conference Series, (in press)
- Jarvis B., Dubath P., Martinet L., Bacon R., 1988, A&AS 74, 513
- Kuijken K., 1993, PASP 105, 1016
- Levison H.F., Duncan M.J., Smith B.F., 1990, ApJ 363, 66
- Martinet L., 1995, Fund. Cosmic Physics 15, 341
- Merrifield M.R., Kuijken K., 1994, ApJ 432, 575
- Pfenniger D., 1993, in: Galactic Bulges, IAU Symp. No. 153, eds. H. Dejonghe, H.J. Habing. Reidel, Dordrecht, p. 387
- Pfenniger D., Friedli D., 1993, A&A 270, 561
- Rix H.-W., Franx M., Fisher D., Illingworth G., 1992, ApJ 400, L5
- Rubin V.C., Graham J.A., Kenney J.D.P., 1992, ApJ 394, L9
- Sellwood J.A., Merritt D., 1994, ApJ 425, 530
- Shaw M.A., Combes F., Axon D.J., Wright G.S., 1993, A&A 273, 31
- Shaw M.A., Axon D.J., Probst R., Gatley I., 1995, MNRAS 274, 369
- Shlosman I., Frank J., Begelman M.C., 1989, Nat 338, 45
- Shlosman I., Begelman M.C., Frank J., 1990, Nat 345, 679
- Tagger M., Sygnet J.F., Athanassoula E., Pellat R., 1987, ApJ 318, L43
- Thakar A.R., Ryden B.S., 1996, ApJ, (in press)
- Wozniak H., Friedli D., Martinet L., Martin P., Bratschi P., 1995, A&AS 111, 115
- Wozniak H., Pfenniger D., 1996, A&A, (submitted)
- Zang T.A., Hohl F., 1978, ApJ 226, 521

This article was processed by the author using Springer-Verlag T_EX A&A macro package 1991.